AD/A-003 346

AN ANALYSIS OF POLAR CAP BACKSCATTER RADAR DATA

Terence J. Elkins

Air Force Cambridge Research Laboratories
Hanscom Air Force Base, Massachusetts

16 September 1974

REPORT DOCUMENTATION PAGE		READ INSTRUCTIONS BEFORE COMPLETING FORM
1. REPORT NUMBER AFCRL-TR-74-C457	2. GOVT ACCESSION NO.	3. RECIPIENT'S CATALOG NUMBER AD/A.003346
4. TITLE (and Subtitle) AN ANALYSIS OF POLAR CAP BACKSCATTER RADAR DATA		5. TYPE OF REPORT & PERIOD COVERED Scientific. Interim.
		6. PERFORMING ORG. REPORT NUMBER AFSG No. 293
7. AUTHOR(s) Terence J. Elkins		8. CONTRACT OR GRANT NUMBER(s)
9. PERFORMING ORGANIZATION NAME AND ADDRESS Air Force Cambridge Research Laboratories (LII) Hanscom AFB Massachusetts 01731		10. PROGRAM ELEMENT, PROJECT, TASK AREA & WORK UNIT NUMBERS Program Element:61102F Proj: 5631 Task 563118 WU: 56311801
11. CONTROLLING OFFICE NAME AND ADDRESS Air Force Cambridge Research Laboratories (LII) Hanscom AFB Massachusetts 01731		12. REPORT DATE 16 September 1974
		13. NUMBER OF PAGES 21
14. MONITORING AGENCY NAME & ADDRESS(if different from Controlling Office)		15. SECURITY CLASS. (of this report) Unclassified
		15a. DECLASSIFICATION DOWNGRADING SCHEDULE

16. DISTRIBUTION STATEMENT (of this Report)

Approved for public release; distribution unlimited.

17. DISTRIBUTION STATEMENT (of the abstract entered in Block 20, if different from Report)

18. SUPPLEMENTARY NOTES

19. KEY WORDS (Continue on reverse side if necessary and identify by block number)

Polar ionosphere
Backscatter radar
HF radio propagation
Ionospheric modelling

20. ABSTRACT (Continue on reverse side if necessary and identify by block number)
    A simplified analysis was performed as a preliminary to a more elaborate analysis of data from an FM/CW backscatter sounder experiment known as RECAP in the polar winter ionosphere. The results show that a reasonably accurate simulation of ionogram data can be achieved with the simple procedure and these results are of value in themselves. A brief survey of the morphology of the polar winter ionosphere is included as an aid

DD _{1 JAN 73} FORM 1473   EDITION OF 1 NOV 65 IS OBSOLETE   Unclassified

1

20. (Contd)

to further data interpretation. Particular attention was paid to the question of clutter, and a model for the different kinds thereof is presented. The suggestion that active control of the antenna radiation pattern may be used to mitigate against clutter degradation in an OTH backscatter radar was examined and found to have merit. Finally, the question of the observed signal strength characteristics was addressed and a model for non-deviative absorption is presented. Further developments await measurement of the RECAP antenna pattern.

Contents

Illustrations

An Analysis of Polar Cap Backscatter Radar Data

I. INTRODUCTION

In the winter of 1973-74 a backscatter radar experiment, designated RECAP, was performed in the polar regions by RADC. This experiment was an extension of the Polar Cap 3 experiment which operated during the preceding year, but differed from Polar Cap 3 principally in that an FM/CW type of HF radar was used instead of a pulse type radar. The RECAP experiment operated in a bistatic mode, with the transmitter at Hall Beach, Canada, and the receiver at Cambridge Bay, Canada. The geometry of the experiment is illustrated in Figure 1, where the location of the Feldstein auroral oval, corresponding to 21 UT is shown in relation to the propagation paths. Also shown are the locations of Alert, where a transponder beacon was located, and of Thule and Resolute Bay. The coordinate system of Figure 1 is the "corrected geomagnetic coordinate" system in which many high latitude ionospheric features are best ordered.
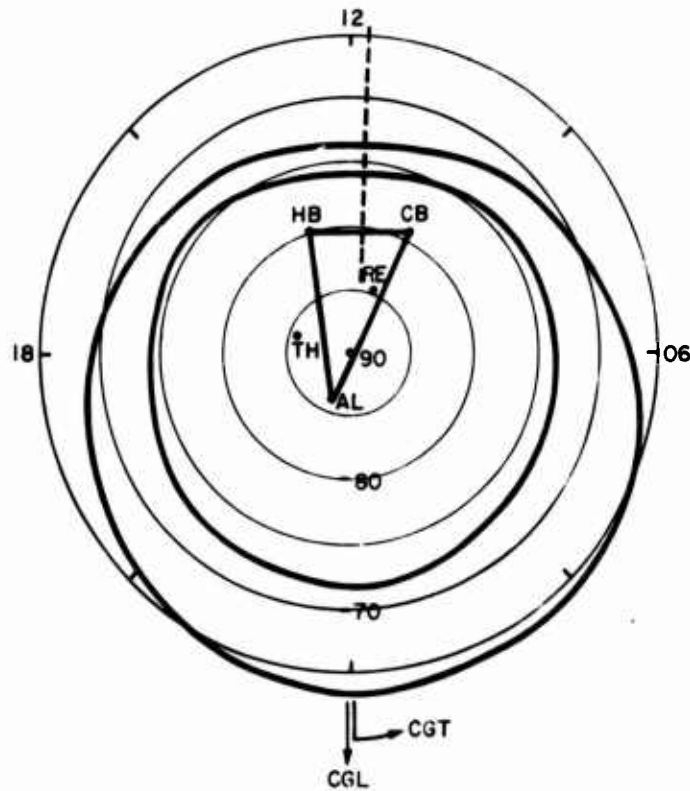
Figure 1. Geometry of the RECAP Experiment at 2100 UT, Showing the Statistical Auroral Oval. HB = Hall Beach; CB = Cambridge Bay; RB = Resolute Bay; TH = Thule; AL = Alert. The dashed line is the perpendicular bisector of HB-CB (see Section 4.2). Coordinates are corrected geomagnetic latitude (CGL) and time (CGT)

The transmitting antenna was the same one as was used in Polar Cap 3, being relatively broad beam, and boresighted in the general direction of the Alert beacon. The receiving antenna was an array of Beveridge elements, having a relatively narrow beamwidth, and oriented towards Alert. In addition to the bistatic back-scatter ionograms obtained in this way, oblique ionograms were also obtained on the direct path from Hall Beach to Cambridge Bay, through the antenna sidelobes. Records were obtained on magnetic tape and a facsimile recorder, and subsequent Doppler processing was performed. This report is concerned specifically with the characteristics of the ionogram records, and represents an attempt to simulate the data using ionosphere and propagation modelling techniques. This is preceded by

6

a brief review of relevant processes which affect the polar ionosphere, which will aid in understanding the morphology of the backscatter data when a more extensive statistical analysis has been performed.

2. MORPHOLOGY OF THE POLAR IONOSPHERE

The dominant temporal variations of the polar ionosphere, as with the temperate ionosphere, is that due to the changing solar zenith angle. However, because of the high latitudes in question, the diurnal and seasonal variations are not as well differentiated as in the temperate latitudes. In summer, when the sun remains continuously above the horizon, the ionosphere is relatively stable, showing little diurnal variation, and relatively little small scale irregularity. In winter, when the only available solar ultraviolet radiation is that scattered from the illuminated hemisphere, the ionization distribution is controlled by energetic particle precipitation and electromotive forces, driven by magnetospheric electric fields.

Sporadic particle precipitation events produce a highly dynamic ionosphere in winter, with rapid spatial and temporal variations in E- and F-region ionization. The topside ionosphere, in particular, is practically always irregular, on a small spatial scale, and this irregularity very often extends downward below the peak of the F-layer. The electric fields of magnetospheric origin which are responsible for plasma drifts also give rise to characteristic variations in the geomagnetic field. There is a correlation between fluctuations in the geomagnetic field and changes in plasma dynamics and structure which, although not well understood, can aid in interpreting certain ionospheric behavior. To a greater extent than anywhere else on the earth's surface, the morphology of the ionosphere and magnetic field in the polar cap reflect conditions in the local interplanetary medium.

Within the polar cap, magnetic field variations are extremely complex, especially during quiet periods, largely because they are the result of several causative mechanisms of roughly comparable magnitude. The magnetic variation pattern during quiet periods appears to show UT and local time dependences, rather than the magnetic time dependence which predominates at auroral latitudes. This behavior is probably due to the variation of the inclination of the geomagnetic axis to the solar wind direction. At Alert, it has been determined[1] that the diurnal magnetic variations which change characteristics between interplanetary magnetic field sectors have a tendency to peak near noon local time (16 UT or 20 MLT). On the Hall Beach-Alert path, this maximum should occur at ~17 UT. During disturbed periods, the pattern becomes better defined, now being dominated by

1. Langel, R. A. and Svalgaard, L. (1974) J. Geophys. Res. 79.

auroral substorm effects, and displays a magnetic local time dependence. The vertical component of magnetic disturbance field during disturbed periods, at magnetic latitudes greater than 80 deg, undergoes reversals at about 08 MLT and 18 MLT.[2] For the Hall Beach-Alert path, these times correspond to about 14 UT and 00 UT respectively. Maximum negative vertical component is at ~19 UT, during periods of auroral substorm disturbance. The morphology of geomagnetic fluctuation is highly relevant to an understanding of high latitude ionospheric variability.

3. AURORAL BACKSCATTER

Diffuse auroral F-region backscatter is observed from a region slightly equatorward of the visible auroral oval — from the region of diffuse optical emissions for which protons may be responsible in the evening sector and diffuse precipitation of electrons in the morning sector. The equatorward boundary of the diffuse backscatter region closely coincides with the boundary of trapped electrons, suggesting a method of monitoring its location by means of satellite measurements of energetic electrons.[3] Greenwald et al,[4] showed that the magnitude of the range integrated backscattered power is proportional to the square of the total horizontal magnetic deflection in a substorm. Discrete auroral echoes are observed poleward of the most poleward occurring visible forms — generally towards the inner boundary of the auroral oval.

The intensity of diffuse echoes may be altitude dependent. Presnell[5] using a frequency of 398 MHz showed that this type of echo originates in the E-region, in particular at a sharp altitude gradient of electron density on the bottomside of the auroral E-layer. It seems likely that these diffuse echoes extend upwards with decreasing intensity, and that an increase in sensitivity due to lower frequencies, in the HF range, accounts for the large F-layer scatter effects at these frequencies. Discrete echoes, on the other hand, do not display any apparent altitude dependence, but seem to originate from a sheet-like reflector of great altitude extent. Diffuse scatter is apparently caused by a plasma instability similar to the two steam instability. The velocity of these diffuse irregularities is comparable to that of neutral

2. Rostoker, G. (1974) Trans. Amer. Geophys. Un. 55:593.

3. Romick, G. J., Ecklund, W. L., Greenwald, R. A., Balsley, B. B., and Imhof, W. L. (1974) J. Geophys. Res. 79:2439.

4. Greenwald, R. A., Ecklund, W. L., and Balsley, B. B. (1973) J. Geophys. Res. 78:8193.

5. Presnell, R. I. (1974) DNA Project 609 Radar: Auroral Backscatter Measurements, DNA 3307F.

winds in the ionosphere (several hundred m/sec). The cause of the discrete type echoes is not known, but their velocity is normally much greater than neutral wind velocities, being usually supersonic (several km/sec).

The frequency dependence of the amplitude of backscatter from diffuse irregularities can be estimated from measured power spectra of electron density fluctuations, which closely follow a power law form over a very large range of transverse scale sizes. Thus,

$$P(f) \sim f^{-2.5}$$

where $P(f)$ is the backscatter power density per ster per Hz and f is the RF. This scaling law can be used to extrapolate approximately from VHF and UHF cross-section measurements. This is useful because the large refraction, broad beam-width and side-lobe levels of practical HF antennas make such measurements difficult in the HF range.

The probability that the two-stream instability will develop, and its intensity when it develops, are proportional to the magnetospheric convection electric field, and thus to the intensity of the auroral electrojet. According to Feldstein,[6] the electrojet intensity maximizes at ~0400 and ~1700 magnetic time. These times are in close agreement with satellite measurements of high latitude magnetic field perturbations.[7] On the basis of such a model, there should be maxima in the diurnal variation of E-region diffuse auroral irregularities at these times — which is well substantiated by VHF and UHF auroral radar studies.[8] These maxima are located 1° to 2° equatorwards of the visible auroral oval. The diurnal variation of diffuse auroral radar clutter at HF is obtained by convolution of the corresponding variation in the occurrence of irregularities together with the diurnal variation of radio refraction. At E-region altitudes, the latter may be assumed small at the higher HF frequencies, so that the irregularity occurrence pattern dominates, leading to maxima at 11 UT (1800 km range) and 23 UT (1100 km range).

6. Feldstein, Y.I. (1969) Rev. Geophys. Space Res. 7:179.

7. Langel, R.A. (1974) J. Geophys. Res. 79:2373.

8. Presnell, R.I., Leadabrand, R.L., Dyce, R.B., Schlobohm, J.C., and Berg, M.R. (1959) SRI Project 2225, Final Report, Part I, RADC-TR-59-34.

4. SIMULATION OF OBLIQUE AND BACKSCATTER IONOGRAMS

In order to investigate the feasibility of simulating the RECAP data using a modelling and ray-tracing technique, a preliminary simplified synthesis has been performed. This work was based on the following assumptions:

1. The ionosphere is spherically symmetric.
2. The local magnetic field is vertical.
3. The vertical F-layer profile is parabolic.
4. Small scale irregularities are distributed isotropically in space.

The ionogram tracing shown in Figure 2a was taken as a typical example (2035 UT on 23 February 1974). Only the leading edge of the scatter trace is reproduced in Figure 2a. The oblique ionogram shows, clearly defined, the ordinary
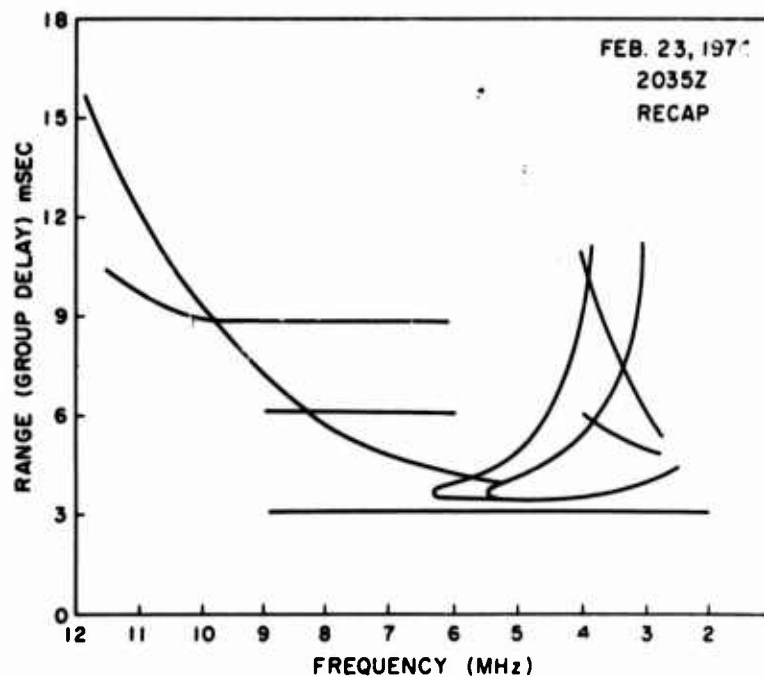
Figure 2a. Observed RECAP Ionograms, Showing Only the Leading Edge of the SF Backscatter. The ground backscatter is below the lower limit of sensitivity of the display

10

and extraordinary lower and upper rays, thus permitting a reliable determination of the ionospheric distribution. Figure 3 shows the equivalent vertical incidence ionogram, derived from the oblique ionogram, based on the "secant law" and taking curvature of the earth and ionosphere into account. Note the sporadic-E layer, and the retardation of the F-trace near the blanketing frequency.

Using the equivalent vertical incidence ionogram as a basis, the 1FGS (ground scatter) trace was computed, by calculating the skip distance for a 1F trace, for a parabolic layer with $y_m/h_m = 0.4$, and plotted in Figure 2b,[9] where

h_m is height of layer maximum, and
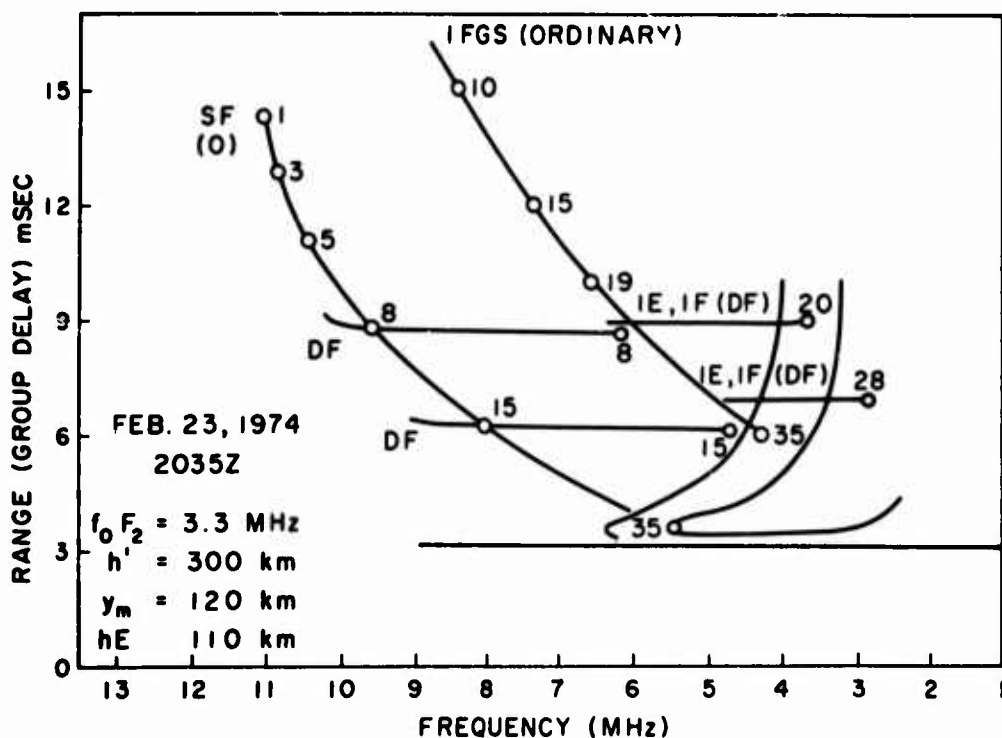
y_m is parabolic semi-thickness.

Figure 2b. Simulated RECAP Ionogram, Corresponding to Figure 2a, Showing Take-off Angles at Selected Points. The ordinary polarization (0) has been computed. The assumed ionospheric parameters are listed

9. Appleton, E. V. and Beynon, W. J. G. (1940) Proc. Phys. Soc. 59:Part II, 58.
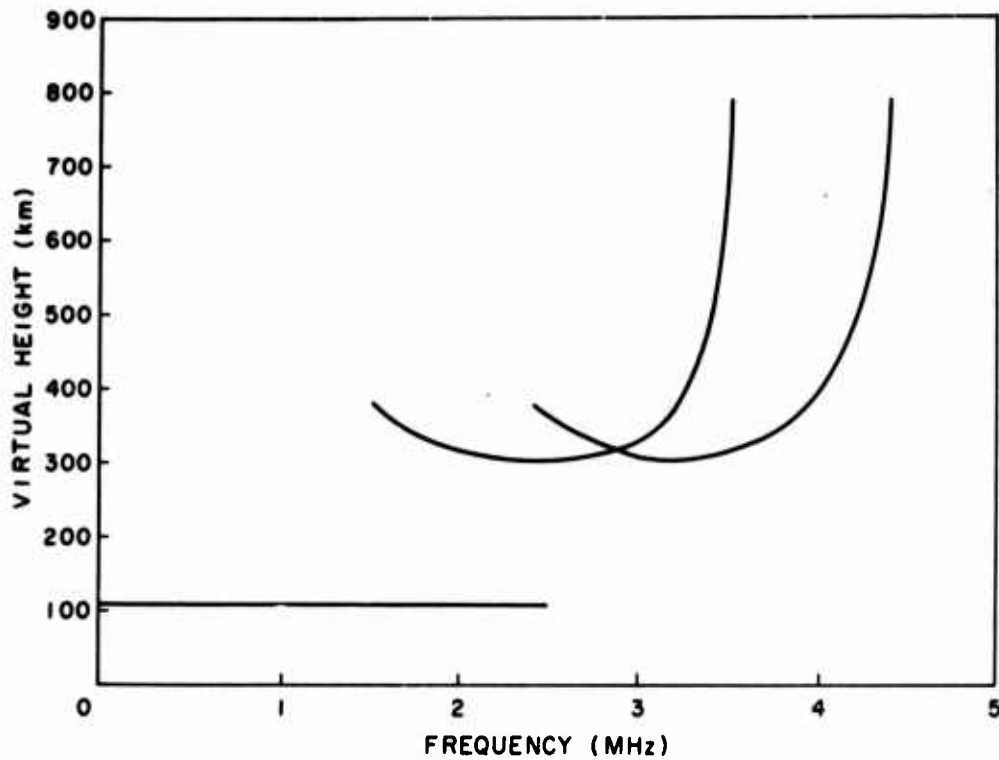
Figure 3. Equivalent Vertical Incidence Ionogram for the Simulation of Figure 2

Figure 4 shows the M-factor (ratio of MUF to foF2) as a function of skip distance for several layer heights. Also shown are several contours of elevation angle of take-off from the transmitter.

4.1 Slant-F

The SF (Slant-F) leading edge trace was computed by making use of the simplifying assumption of vertical geomagnetic field. For a symmetric ionosphere, this assumption implies that SF is observed at half the range of the ground, for a particular take-off angle. The leading edge is therefore established as half the skip distance for a particular frequency. SF at all greater ranges than that of the leading edge is scattered at take-off angles less than the maximum value required for the leading edge trace.
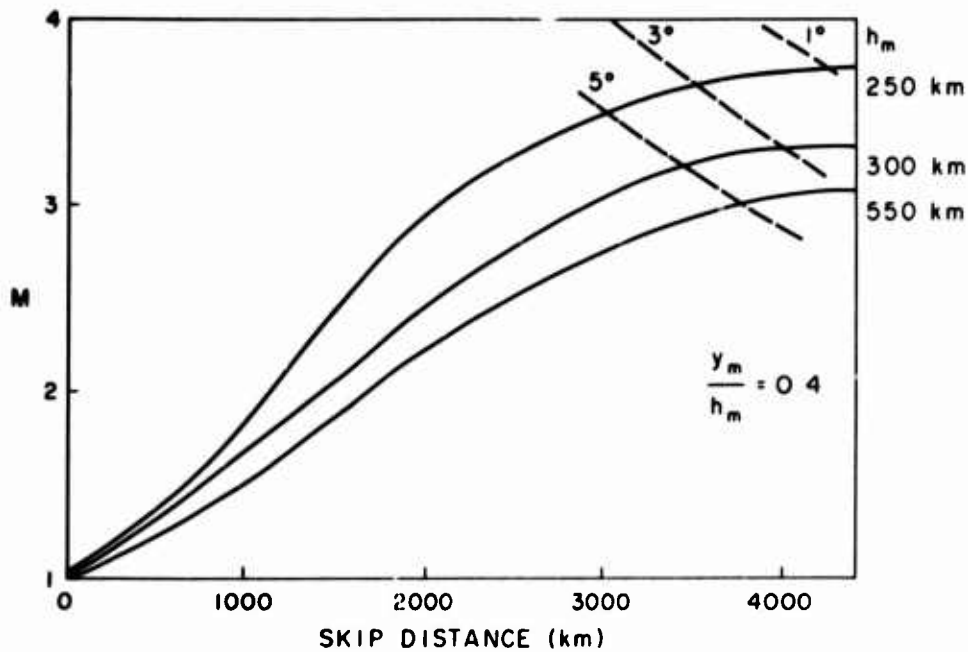
12

Figure 4. Variation of M Factor With Skip Distance for Some Representative Ionospheric Conditions; Dashed Lines are Antenna Take-off Angles

4.2 Direct-F

The direct-F traces are assumed to result from backscatter of radar energy from overdense field-aligned sheets of ionization extending over a large altitude range in the auroral ionosphere. These sheets are observed sporadically and there is no a priori knowledge as to their location. There is reason to believe that they are closely associated with visible auroral arcs, which are usually located within the bounds of the statistical "auroral oval", deduced by Feldstein.[6] These sheets of ionization are so large and so intense that they constitute very large targets, even then viewed through the side and back lobes of the antennas. It is not valid to assume that DF echoes are due to irregularities located within the main beam coverage of the radar. However, the simplifying assumptions which were made permit a reasonably confident estimate of their location. With the relatively large baseline of the bistatic RECAP experiment, surfaces of constant group path delay form fairly elongated ellipsoids, with the transmitter and receiver at the foci. The assumptions of spherical symmetry and vertical magnetic field result in the constraint that the radar is most sensitive to discrete irregularities located on a horizontal section through this ellipsoid, along a line forming the perpendicular bisector of the baseline (two points). If the DF-producing irregularities are assumed to

13

be confined to the auroral oval, it will be shown shortly that one of these possible points is eliminated for practical purposes, and that most of the observed DF is seen in the antenna back'obes. Figure 5 shows the UT dependence of the range (expressed as group delay) to the inner and outer boundaries of the auroral oval, under average geomagnetic activity, for the RECAP geometry.
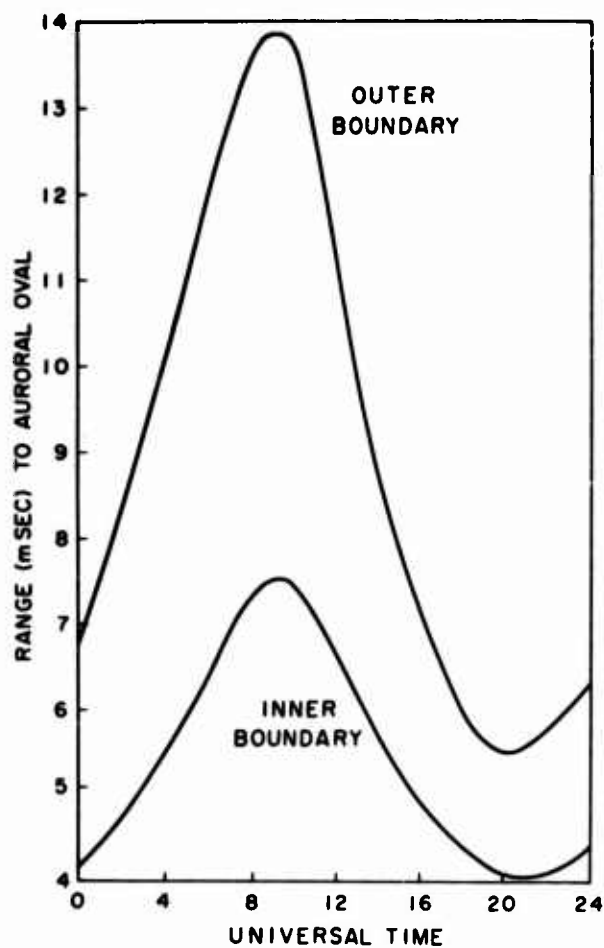

Figure 5. Range to the Inner and Outer Boundaries of the Statistical Auroral Oval, for the RECAP Experiment

14

The most intense and most frequently occurring auroral irregularities (of the discrete or DF-producing type) are expected to occur in the post-midnight auroral break-up period (between midnight and 03 local magnetic time). For the location and geometry of the RECAP experiment, this period would be centered at about 08 UT, with a corresponding echo range of 7.5 - 14 msec.

On the basis of the foregoing considerations, computations were made of the DF contributions to the synthesized ionogram, considering two auroral sheets located in the auroral oval at appropriate ranges. Because of the assumed large vertical extent of the sheets, these traces cover a large frequency range with very little group retardation. The lower frequency limit of the traces is due to the blanketing effect of the underlying sporadic-E ionization, assuming that the secant law applies, as seems reasonable.

In addition to the simple DF computation, additional traces were computed for multiple hop DF modes, namely those in which the radar energy undergoes an intermediate E-hop before scattering from the same two auroral sheets in the F-region. This results in traces at slightly longer group delay, and confined to lower frequency ranges, because of the greater take-off angles required. These traces would not necessarily be observed in the standard ionogram display because of its limited dynamic range (~10-15 dB). Since they undergo four more D-region penetrations than the 1FDF traces, their intensity would be typically 20 dB below that of the 1FDF traces, to which the display is effectively normalized. Clearly many other combination modes are possible, and it is useful to imagine an ionogram display of very large dynamic range being fairly densely filled by such lower intensity traces. It should be noted that DF traces are expected to occupy a narrow Doppler range, since the discrete sheets producing them are moving coherently. Consequently, the proliferation of low level DF traces may not be too serious, from a target detection viewpoint, even though the Doppler offset of all traces may be different, due both to the different characteristic velocities of different sheets, and the different radial components of different modes.

The abrupt cut-off at the low frequency end of the DF traces is due to the shielding of the F-layer at frequencies below the sporadic-E blanketing frequency at the particular oblique range involved. The upper frequency cut-off is due to penetration of either the F or sporadic-E layer for this particular case, whichever has the lower penetration frequency.

4.3 Take-Off Angle

The composite synthesized ionogram in Figure 2b is labelled at some representative points with values of the antenna take-off angle corresponding to those points. An important consideration is to note that, although the SF diffuse trace

15

extends back through the ground trace, and several DF traces penetrate it, the resulting masking of the ground trace can be reduced by control of the vertical antenna radiation pattern. Specifically, by introducing low angle cut-off, it should be possible to enhance target visibility against SF clutter. Discrimination against DF obscuring clutter can be achieved by null-steering in the vertical plane of the side and back lobes, or by horizontal control of the antenna pattern.

5. SIGNAL ABSORPTION

Measurements of radar signal loss, using the Alert beacon, have been summarized in the reports on the Polar Cap 3 experiment in almost the same ionospheric region as RECAP was performed. These have revealed the following general features:

    1. F-mode losses exceed E-mode losses, typically by 10-20 dB.

    2. Losses have a seasonal dependence, so far as can be determined from data currently available.

    3. In summer, when the ionosphere is most stable, 2-way E-mode losses exceed space losses by about 20 dB.

It is necessary to explain these observations, and of special interest to account for the excess of F-mode losses over E-mode losses. This has been attempted by modelling the expected signal absorption and making use of some available RECAP data.

D-region (non-deviative) absorption has been measured at numerous locations for many years, using the vertical reflection technique. In particular, observations have been reported at 2 MHz, vertical incidence, [10] from Resolute Bay (74.7°N; 94.9°W). Wakai and Watanabe[11] have modelled the non-deviative component of absorption, based on data of this kind, as

$$L = A \cos^n \chi$$

where L (dB) is the two-way vertical absorption

χ is the local solar zenith angle,

A, n are constants having a geographic latitude dependence.

10. Davies, K. (1960) J. Geophys. Res. 65:2285.
11. Wakai, N. and Watanabe, S. (1961) J. Radio Res. Labs. 8:413.

Although not considered by Wakai and Watanabe, A may also have a seasonal variation due to thermospheric composition changes with season (the "winter anomaly"), but this additional variation may not be important at very high latitudes.

Taking values of A = 30, n = 0.05 for a geographic latitude of 80°, a solar zenith angle dependence is obtained as shown in Figure 6. In addition to a 2 MHz curve, similar curves for several other frequencies are plotted, for the oblique path to Alert, based on a frequency scaling law[12]

$$L \sim f^{-1.6}.$$

where f is frequency. Note that, because of the small value of n, the dependence on solar zenith angle is very weak for solar elevation angles appreciably above horizon grazing incidence. A typical value for two-way attenuation at 9 MHz is 10 dB.
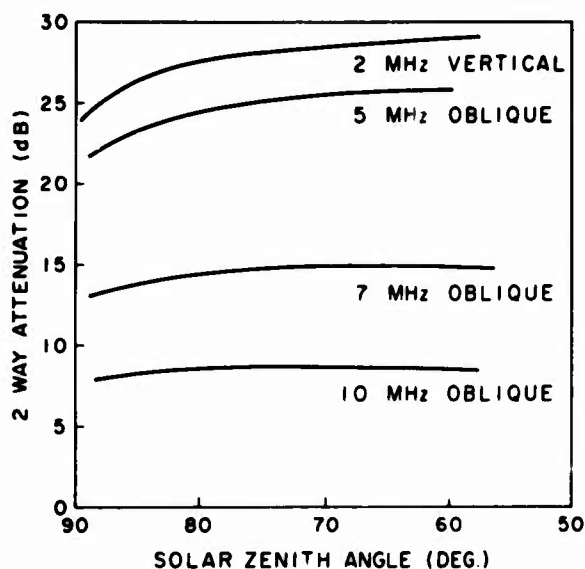

Figure 6. Attenuation as a Function of Solar Zenith Angle and Frequency for Vertical Incidence (at 2 MHz) and for Oblique Incidence on the RECAP-Alert Path

12. Khodza-Alchmedov, Ch. L. (1965) Geomag. and Aeron. 5:59.

The RECAP experiment involved making relative signal amplitude measurements of the Alert beacon return. An example is shown in Figure 7, where multiple mode structure is clearly in evidence, with differences in group path delay of about 0.2-0.3 msec. By means of the simplified ray-tracing technique already described, these modes have been identified as follows, where the angle of take-off from the antennas on both paths is included, as well as the signal strength relative to the dominant mode:

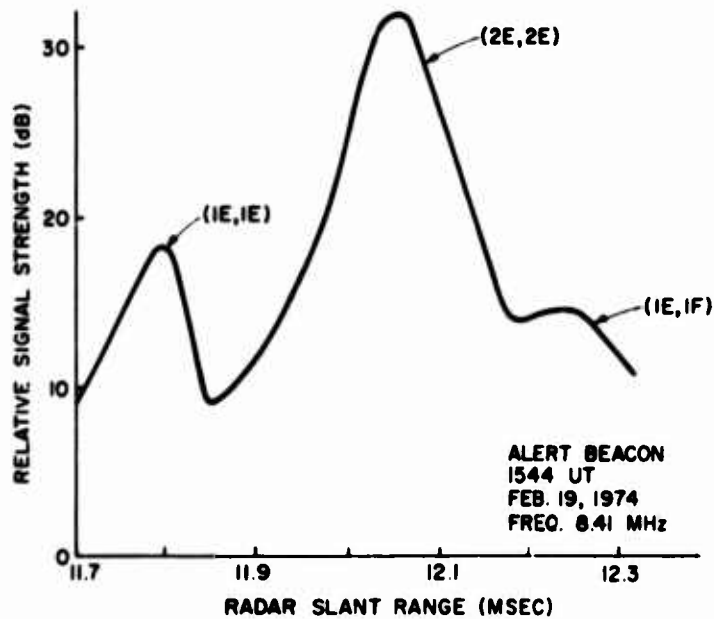| Case	Mode	Relative Signal Strength (dB)	Group Delay (msec)	Take-off Angle
(a)	2E, 2E	0	12.05	13.4°, 10.6°
(b)	1E, 1E	-13.8	11.80	4.1°, 2.2°
(c)	1E, 1F	-17.5	12.25	4.1°, 15.5°

Figure 7. Measured Relative Signal Strength, Showing Multimode Structure, Where the Modes are Identified by Modelling and Ray Tracing

18

By taking into account the variation of absorption with D-region incidence angle, as determined from the model and the measured loss differential corresponding to differing numbers of D-region penetrations, the two-way absorption at 8.41 MHz vertical incidence can be estimated. When the antenna radiation patterns are available, it will be possible in this way to estimate the magnitude of the loss in excess of that due to absorption, and also its distribution between E- and F-region reflections.

The discrepancy noted between signal strengths for E- and F-modes can tentatively be taken to be associated with the region of the ionosphere above the E-region. Calculations of deviative absorption show that the loss due to electron-ion collisions in the F-region, for a two-way path, is unlikely to exceed 2-3 dB. The tentative conclusion is that the excess loss is due to scattering in the F-layer. The polar F-layer is known to be highly irregular on a small scale, so that such a conclusion appears not unreasonable. Further analysis will reveal whether any characteristic diurnal or seasonal variations can confirm this conclusion.

6. SUMMARY

One of the purposes of the RECAP experiment was to improve our understanding of the HF propagation characteristics of the polar ionosphere, specifically as they influence the performance of backscatter radars. A brief review of certain relevant morphological features has been presented with the aim of providing a basis for ordering the diurnal and other notable variations which have been observed in preliminary analysis of the data. Then, by using a simple modelling and propagation simulation procedure, it was shown that the main features of a typical RECAP ionogram could be reproduced. Although this work is but a preliminary to a more elaborate simulation analysis, employing three dimensional ionospheric modelling and ray tracing, the results are themselves sufficiently encouraging to merit serious attention.

Special attention has been devoted to the question of ionospheric (and auroral) clutter, likely to be a major factor in performance of a high latitude OTH-B radar. The necessary take-off angles at the radar antennas to generate clutter at particular range-frequency combinations have been computed. On this basis, a potential method for clutter mitigation has been evaluated, in which control of the antenna radiation patterns is the key ingredient. Some consideration has also been given to the observed signal strength, in particular to the question of the source of the apparent excess of F-mode losses over E-mode losses. A model for the non-deviative absorption has been presented and an attempt made to explain some actual data. The completion of this analysis must await the measurement of both antenna radiation patterns.

19

References

1. Langel, R. A. and Svalgaard, L. (1974) J. Geophys. Res. 79.

2. Rostoker, G. (1974) Trans. Amer. Geophys. Un. 55:593.

3. Romick, G. J., Ecklund, W. L., Greenwald, R. A., Balsley, B. B., and Imhof, W. L. (1974) J. Geophys. Res. 79:2439.

4. Greenwald, R. A., Ecklund, W. L., and Balsley. B. B. (1973) J. Geophys. Res. 78:8193.

5. Presnell, R. I. (1974) DNA Project 609 Radar: Auroral Backscatter Measurements, DNA 3307F.

6. Feldstein, Y. I. (1969) Rev. Geophys. Space Res. 7:179.

7. Langel, R. A. (1974) J. Geophys. Res. 79:2373.

8. Presnell, R. I., Leadabrand, R. L., Dyce, R. B., Schlobohm, J. C., and Berg, M. R. (1959) SRI Project 2225, Final Report. Part I, RADC-TR-59-34.

9. Appleton, E. V. and Beynon, W. J. G. (1940) Proc. Phys. Soc. 59:Part II, 58.

10. Davies, K. (1960) J. Geophys. Res. 65:2285.

11. Wakai, N. and Watanabe, S. (1961) J. Radio Res. Labs. 8:413.

12. Khodza-Alchmedov, Ch. L. (1965) Geomag. and Aeron. 5:59.

Preceding page blank